Graphene-based Symmetric and Non-Symmetric Magnetoresistive Junctions

Hashmi, Arqum

Nakanishi, Kenta

Ono, Tomoya

(Citation)
Journal of the Physical Society of Japan,89(3):034708

(Issue Date)
2020-03-15

(Resource Type)
journal article

(Version)
Accepted Manuscript

Graphene-based symmetric and non-symmetric magnetoresistive junctions

Arqum Hashmi,[1] Kenta Nakanishi,[2] Tomoya Ono [3†]*

[1] Center for Computational Sciences, University of Tsukuba, Tsukuba, Ibaraki 305–8577, Japan

[2] Graduate School of Pure and Applied Sciences, University of Tsukuba, Tsukuba, Ibaraki 305–8571, Japan

[3] Department of Electrical and Electronic Engineering, Kobe University, Kobe 657–8501, Japan

ABSTRACT

First-principles investigations combined with the nonequilibrium Green's function method are conducted to understand the spin-polarized transport property in graphene (Gr) based magnetic tunnel junctions (MTJs). Our systematic and comparative investigation is not only restricted to junctions with Ni electrodes on both sides (symmetric junctions) but also the junctions where one side is Ni and the other is Co (non-symmetric junctions). The spin-resolved density of states and k-resolved transmission spectrum are analyzed to show tunneling behavior. In spite of low magnetic exchange couplings between the electrodes, spin filtering is quite sensitive to electrode material. Distinct hybridization of the Gr π states with symmetric and non-symmetric junctions is observed. Gr based junctions display higher transmission spectra indicating low contact resistance irrespective of the electrode material. Furthermore, the influence of different stacking of electrode layers on transport properties is also checked. Tunneling magnetoresistance ratios of Gr-based MTJs are drastically affected by the Fermi surfaces of electrodes. Both symmetric and non-symmetric junctions exhibit distinctive selection rules due to the incompatibility of wave functions of electrodes on both sides of the interface. Our present work reveals the importance of electrode materials for Gr-based MTJs, which may be used to design next-generation spintronics applications.

I. INTRODUCTION

Study on two-dimensional (2D) materials has drawn increasing interest owing to their extraordinary physical properties. Examples mainly include graphene (Gr)[1], hexagonal boron nitride (h-BN)[2], transition-metal (TM) dichalcogenide[3], and phosphorene[4] because of their unique potentials in electronics. Despite the fact that these 2D materials show no intrinsic magnetism in ideal structures, active research has been focused on using these 2D materials for spintronics applications. A magnetic tunnel junction (MTJ)[5] consists of a nonmagnetic spacer region between two ferromagnetic TM electrodes with variable magnetization direction. Many 2D materials have attracted great interest as promising candidates for spacer region in MTJs[6]. Spin-polarized transport of hot electrons[7] is greatly affected by the spacer material in MTJs. From an experimental point of view, spin-polarized transport perpendicular to the interface has a certain advantage over the in-plane current configuration[8].

The tunneling magnetoresistance (TMR) ratio has been directly observed in experiments and is the most important feature of MTJs. In principle, the "optimistic" definition of the TMR ratio is

$$TMR = \frac{(G_P - G_{AP})}{G_{AP}} \times 100\% \approx \frac{(G_{\uparrow\uparrow} + G_{\downarrow\downarrow} - 2G_{\uparrow\downarrow})}{2G_{\uparrow\downarrow}} \times 100\%,$$

where $G_{\uparrow\uparrow}$ and $G_{\downarrow\downarrow}$ are spin resolved quantum conductances of majority and minority spins in parallel configuration (PC) of magnetization, respectively, while $G_{\uparrow\downarrow}$ is quantum conductance in antiparallel configuration (APC). The G_P (G_{AP}) is total conductance in PC (APC). It is important to achieve a high TMR ratio while maintaining reasonably low electric resistance for promoting practical application of MTJs. The TMR is quite sensitive to the atomic and chemical composition of the interface structure, and achieving a high TMR ratio is often restricted by the inability of obtaining well-ordered interfaces[10,11] between electrodes and the spacer region. Hence, intrinsically high-quality interfaces are important for spin-polarized transport through MTJs. Semi-metallic Gr is promising material for the spacer region because Gr layer have been grown epitaxially on a broad range of metallic substrates[12–14]. Moreover, the quality of such epitaxial layer is very high and the covalent bonds between carbon atoms of Gr sheet is preserved while grown on metal surfaces. This excellent combination may provide a platform for novel next-generation nanoscale devices.

Previous reports on MTJs using Gr spacer region are mostly limited to symmetric junctions in which both electrodes are the same material [15–19]. Our investigation includes symmetric junctions, both electrodes are Ni, and non-symmetric junctions, one is Ni and the other is Co and Gr monolayer (ML) is used as covalently bonded spacer. There are several key reasons to choose these junctions: First, the lattice mismatch among Ni(111), Co(111), and Gr is small (≈1.3%). Second, the electronic states of Gr at the Fermi level are mainly located at high symmetry K point in reciprocal space,

while only minority-spin states of Ni(111) and Co(111) exist at the K point[16–18], which gives rise to a high TMR ratio. Last but not least is weak spin-orbit interaction implied by the low atomic number of C atoms. This weak spin-orbit coupling translates into long spin-flip scattering length, which is desirable in the field of spintronics.

II. NUMERICAL METHOD

The Vienna ab initio simulation package (VASP)[21,22] is used to obtain optimized interface geometries, spin-resolved density of states (DOS), magnetic moments, and interlayer magnetic exchange coupling for MTJs within the framework of density functional theory (DFT). Valence electrons are treated explicitly and their interactions with ionic cores are described by projector augmented wave method[23]. The exchange-correlation interactions are approximated by local density approximation (LDA)[24]. All results are obtained with high plane-wave cut-off energy of 700 eV. The convergence criteria for energy and force are set to 10^{-7} eV and 0.001 eVÅ^{-1}, respectively.

For the transport calculations, we use the nonequilibrium Green's function method based on DFT. All the electron transport calculations are carried out using RSPACE code[25–29] which is based on the real-space finite-difference method[30,31]. Exchange-correlation interactions are treated by LDA, and the norm-conserving pseudopotentials[32] of Troullier and Martins[33] are used for the core electrons with a grid spacing of 0.15 Å. The relative spin directions of two electrodes are changed to obtain zero bias-dependent transmission for both PC and APC. After self-consistent calculations of the device, the spin-polarized tunneling conductance is obtained using the Landauer formula[34].

$$G^{\sigma} = \frac{e^2}{h} \sum_{k_{||}} T_{\sigma}\,(k_{||}, \epsilon)$$

with $\sigma \equiv \uparrow, \downarrow$ being the spin index, and $T_{\sigma}(k_{||}, \epsilon)$ the spin dependent transmission probability at the energy ϵ with $k_{||} = (k_x,\ k_y)$.

III. NUMERICAL RESULTS

We first describe the geometry and stacking order of the MTJs. Figure 1(a) [1(b)] shows the schematic illustration of Gr spacer region between two different types of electrodes. The atomic models for vertical stacking order of Gr junctions are shown in Figs. 1 (c) and 1(d), respectively. The lateral length of the supercell is 1×1 of face-centered cubic (fcc)-(111) with an in-plane lattice constant of 2.46 Å. We neglect the small lattice mismatch between electrodes and spacer region at the interfaces. The integration in the Brillouin-zone (BZ) is carried using Monkhorst-Pack k-point

sampling with a 24×24×1 k-mesh. A vacuum region of 15 Å is inserted in the z direction. Since an important phenomenon take place at the interface region, the atomic geometries in the three atomic layers adjacent to the Gr spacer region are allowed to relax in the vertical directions. The total energies of all possible stacking orders of electrodes are calculated separately and the lowest-energy structures of all systems are summarized in Table I. Gr display short bond lengths of 2.06–2.08 Å for each side of the interface, which is in good agreement with the experimental value of 2.16±0.10 Å[35,36]. It has been widely reported that Gr layer is chemisorbed on Ni(111) and Co(111) surfaces[17,37], and our study is consistent with these reports. In these junctions, a pronounced buckling feature with a relative height difference of ~0.15 Å is observed in the Gr layer. The buckling feature found in the Gr does not depend on the junction type (symmetric or non-symmetric). The stacking order in the ML of the Gr is independent of the electrode material.

TABLE I: Lowest-energy atomic structures, interlayer exchange couplings ($\Delta E = E_P - E_{AP}$), spin-resolved quantum conductances of majority-spin ($G_{\uparrow\uparrow}$), minority-spin ($G_{\downarrow\downarrow}$), APC ($G_{\uparrow\downarrow}$), and TMR ratios. Notation for stacking order is identical to that in Figure 1. a, b and c correspond to A, B and C layers of fcc(111), respectively. A (B) site of 2D sheets indicates alignment of a(b) and c(a) sites of fcc(111).

Junction	Stacking order	$\Delta E = E_p - E_{AP}$ (meV)	$G_{\uparrow\uparrow}$	$G_{\downarrow\downarrow}$	$G_{\uparrow\downarrow}$	TMR ratio (%)
Ni/vacuum/Ni	cba |A| cba	-	3.28	5.70	4.35	3.30
Ni/Gr(ML)/Ni	cba |A| cba	9	17.40	19.30	16.20	13.60
Co/vacuum/Ni	cba |A| cba	-	3.8	4.89	4.02	8.26
Co/Gr(ML)/Ni	cba |A| cba	35	18.10	15.50	16.70	8.26

Next, we describe the magnetic and electronic properties of MTJs. The interlayer exchange coupling is calculated by taking the energy difference between PC and APC ($\Delta E = E_P - E_{AP}$) with E_P and E_{AP} being the total energy of PC and APC, respectively. APC is energetically favored and independent of the junction type. Moreover, both junctions show

relatively small energy difference between PC and APC, resulting in the magnetic bi-stability in current systems. This finding indicates that the interaction between two electrodes is negligible; thus, it will be easy to tune the relative magnetization of two electrodes. Figure 2 shows the spin-resolved DOS of ML junctions for the most stable spin configurations. An ordinary metallic behavior appears in Gr as shown in Fig. 2(b). This observation shows the strong hybridization between the electronic states of Gr and electrodes at the interface. Figures 2(a) and 2(c) show that the DOS of one spin in the interface layers of the Ni(111) [Co(111)] electrode is suppressed at the Fermi level compared to other spins. Thus, TM layers at interface show a weak half-metallic state. Note that no meaningful disparity is found in the DOS irrespective of symmetric and non-symmetric junction. Figure 2(d) shows the projected band-structure of Gr layer sandwiched between TM and a typical Dirac cone of Gr is not preserved upon the formation of MTJ. As one can see from the projected band, the Gr derived π states near the Fermi level hybridize significantly with the dz^2 orbital of the Ni and Co surfaces. π states (bonding and antibonding) of Gr have distinctive hybridization with electrodes for symmetric and non-symmetric junctions near the Fermi level. This finding indicates that both junctions will exhibit different conductance behavior and consequently it will affect the TMR ratios for symmetric and non-symmetric junctions. Ni shows a magnetic moment in the range of 0.3–0.6 μ_B while Co has the magnetic moments of 1.2–1.6 μ_B inside the Wigner-Seitz radius. As shown in Figs. 2(a)–2(c), the magnetic state is found in the Ni and Co electrodes, and no meaningful spin polarization is observed in the spacer region. Very small magnetic moments in the range 0.01–0.03 μ_B per atom are observed in the spacer region and this is independent of the relative magnetization direction of electrodes. In the non-symmetric junctions, the magnetic moment of Co is much larger than that of Ni, indicating that the induced magnetic moment in the spacer region is mostly affected by the Co electrode.

We further investigate the spin-dependent transport properties at zero bias. Figure 3 shows a schematic illustration of two-terminal MTJ device containing electrodes and scattering part for the Gr spacer region. The two-terminal structure is divided into three regions: left electrode, right electrode, and the scattering region. The MTJ structure is periodic in the *x*-*y* directions, and the transport is calculated perpendicular to the plane in the *z*-direction. The scattering region contains 28 atoms, including three electrode layers on both sides of the spacer region. The k-space integrations are carried out with 4 × 4 × 1 k-points. Table I presents the TMR ratio for each junction, and we can infer the following information. We have also checked the influence of different stacking of electrode layers on transport properties and it will be discussed later. The symmetric junction has higher TMR ratio compared to non-symmetric junction. The highest TMR ratio observed in symmetric junction is 13.60%, while it is 8.26% in non-symmetric Gr based junction.

The spin-dependent transmission spectra are shown in Fig. 4 in the form of the conductances in PC [$G_{\uparrow\uparrow}$ (Majority-spin) and $G_{\downarrow\downarrow}$(Minority-spin)] and in APC ($G_{\uparrow\downarrow}$). Figures 4(a) and 4(b) show the transmission spectra of symmetric and non-symmetric junctions through a vacuum gap. We found that both systems containing vacuum gap show quite different quantum conductances in Figs. 4(a) and 4(b), therefore TMR ratios differ in both junctions. Although the $G_{\downarrow\downarrow}$ is much larger than $G_{\uparrow\uparrow}$ in both systems. This is obvious because both Ni and Co have large DOS of minority-spin states at Fermi level as compared to majority-spin. Pristine Gr is essentially transparent for both spin channels. Upon the introduction of Gr ML, the electronic states of Gr strongly couple with metal d-states, destroying their original characteristics and resulting in a dramatic increase in the transmission coefficient, as shown in Figs. 4(c) and 4(d). The transmission spectra of Gr based junctions have larger conductance values than junctions with vacuum gap at the Fermi level and all spin channels participate in conductance. From symmetric to non-symmetric junctions, $G_{\uparrow\uparrow}$ becomes dominant over $G_{\downarrow\downarrow}$, which results in a low TMR ratio. $G_{\uparrow\downarrow}$ is lower in symmetric junctions than non-symmetric junctions and this is the one of the reason of having different TMR ratios in both types of junctions. Our results are close to those from previous reports on Gr-based symmetric junctions [16,20]. Since the transmission spectrum is not only interrelated with the electronic structure but also determines the current value, the Gr based junctions display higher transmission spectra than vacuum based region indicating low contact resistance irrespective of the electrode material. Stacking faults are most common in metals with fcc structure, so we have also checked the effect of different stacking of electrode layers. Gr based junctions is affected more than junctions containing vacuum gap by the different stacking of electrode although the difference in conductance is quite small. As one can see in Fig.4 that the conductance spectrum for different stacking order for TM electrode does not affect much the transport properties so hence afterwards we will just show the results for most stable stacking order.

To understand the calculated quantum conductances and the resulting magnetoresistance ratios, we analyzed the k-resolved $k_{||} = (k_x, k_y)$ conductance spectra. The reciprocal lattice for the rectangular unit cell of Gr is shown in Fig. 5. The k-resolved spectra is calculated on different k-points of the rectangular unit cell are indicated by k-1~k-6, while those corresponding to reciprocal lattice of the hexagonal unit cell are indicated by Γ, M and K. Figures 6 and 7 show the $k_{||}$ conductance spectrum for majority and minority spins respectively. The majority-spin conductance $G_{\uparrow\uparrow}$ in the PC does not show any change in both symmetric and non-symmetric junctions through a vacuum gap. Even upon constructing the Gr ML junctions, $G_{\uparrow\uparrow}$ undergoes little change except it is just shifted to higher values. This behavior stems from the similarity of the corresponding majority-spin Fermi surfaces of the Ni(Co)-(111) surfaces, which are

formed by partially filled *s* bands. However, much larger differences are found for $G_{\downarrow\downarrow}$ involving the minority-spin which is reflected by the drastically different Fermi surfaces[21] of Ni and Co resulting from the interplay between *s* and *d* states. This displays distinctive selection rules due to the incompatibility of wave functions of electrodes on both sides of the interface for symmetric and non-symmteric junctions. In the presence of Gr ML, $G_{\downarrow\downarrow}$ shows entirely different k-resolved conductance and this can be attributed to the distinct hybridization of the π states of Gr in symmetric and non-symmetric junctions. Overall, the Gr exhibit conducting behavior for both majority and minority spins irrespective of the electrode material. Large transmission due to Bloch states of $G_{\downarrow\downarrow}$ is coming throughout the BZ while $G_{\uparrow\uparrow}$ transmission depends on particular $k_{||}$ where the gap between Gr π and Ni(Co) states is small. To this end, it should be emphasized that the choice of electrode material plays a vital role for developing Gr based high TMR ratio device.

IV. Summary

We investigated the structural, magnetic, and spin-dependent transport properties of MTJs, in which Gr layer is sandwiched between ferromagnetic electrodes. Typical Dirac cone feature of Gr is not preserved upon the formation of MTJ and Gr derived π states near the Fermi level was strongly hybridized with the dz^2 orbital of the Ni and Co surfaces. APC was found to be stable in the Gr-based ML junctions and distinct hybridization of the Gr π states are observed with symmetric and non-symmetric junctions. Spin filtering is quite sensitive to the electrode materials. The symmetric junction has higher TMR ratio compared to non-symmetric junction. The highest TMR ratio observed in symmetric junction is 13.60%, while it is 8.26% in non-symmetric Gr based junction. Gr based junctions displayed the higher transmission spectra indicating low contact resistance irrespective of the electrode material. Furthermore, the influence of different stacking of electrode layers on transport properties is also checked although not much difference is observed in conductance spectra. Both symmetric and non-symmetric junctions exhibit distinctive selection rules due to the incompatibility of wave functions of electrodes. Our comparative study reveals the effect of various electrode materials on spin transport property that can help to develop Gr-based high TMR ratio devices.

AUTHOR INFORMATION

Corresponding Author

*E-mail: hashmi.arqum.ga@u.tsukuba.ac.jp, †E-mail: ono@ccs.tsukuba.ac.jp

ACKNOWLEDGMENTS

This research was partially supported by MEXT as a social and scientific priority issue (Creation of new functional devices and high-performance materials to support next generation industries) to be tackled by using post-K computer, JSPS KAKENHI Grant No. 19K15381, and JSPS Core-to-Core program (Controlled Interfacing of 2D materials for Integrated Device Technology). The numerical calculations were carried out using the computer facilities of the Institute for Solid State Physics at the University of Tokyo, the Center for Computational Sciences at University of Tsukuba, and the K computer provided by the RIKEN Advanced Institute for Computational Science through the HPCI System Research project (Project ID: hp180226).

References

[1] K.S. Novoselov, A.K. Geim, S.V. Morozov, D. Jiang, Y. Zhang, S.V. Dubonos, I.V. Grigorieva, and A.A. Firsov, Science **306**, 666 (2004).
[2] K. Watanabe, T. Taniguchi, and H. Kanda, Nature Materials **3**, 404 (2004).
[3] X. Xu, W. Yao, D. Xiao, and T.F. Heinz, Nature Physics **10**, 343 (2014).
[4] L. Li, Y. Yu, G.J. Ye, Q. Ge, X. Ou, H. Wu, D. Feng, X.H. Chen, and Y. Zhang, Nature Nanotechnology **9**, 372 (2014).
[5] M. Julliere, Physics Letters A **54**, 225 (1975).
[6] T. Song, X. Cai, M.W.-Y. Tu, X. Zhang, B. Huang, N.P. Wilson, K.L. Seyler, L. Zhu, T. Taniguchi, K. Watanabe, M.A. McGuire, D.H. Cobden, D. Xiao, W. Yao, and X. Xu, Science eaar4851 (2018).
[7] T. Banerjee, W.G. van der Wiel, and R. Jansen, Phys. Rev. B **81**, 214409 (2010).
[8] Z.H. Ni, H.M. Wang, Y. Ma, J. Kasim, Y.H. Wu, and Z.X. Shen, ACS Nano **2**, 1033 (2008).
[9] L.H. Li and Y. Chen, Advanced Functional Materials **26**, 2594 (2016).
[10] P.X. Xu, V.M. Karpan, K. Xia, M. Zwierzycki, I. Marushchenko, and P.J. Kelly, Phys. Rev. B **73**, 180402 (2006).
[11] Z. Ebrahiminejad, R.S. Dariani, and S.F. Masoudi, Electron. Mater. Lett. **10**, 573 (2014).
[12] J. Gao, J. Yip, J. Zhao, B.I. Yakobson, and F. Ding, J. Am. Chem. Soc. **133**, 5009 (2011).
[13] E. Cazzanelli, T. Caruso, M. Castriota, A.R. Marino, A. Politano, G. Chiarello, M. Giarola, and G. Mariotto, Journal of Raman Spectroscopy **44**, 1393 (2013).
[14] B. Wang and M.-L. Bocquet, J. Phys. Chem. Lett. **2**, 2341 (2011).
[15] V.M. Karpan, G. Giovannetti, P.A. Khomyakov, M. Talanana, A.A. Starikov, M. Zwierzycki, J. van den Brink, G. Brocks, and P.J. Kelly, Phys. Rev. Lett. **99**, 176602 (2007).
[16] K.K. Saha, A. Blom, K.S. Thygesen, and B.K. Nikolić, Phys. Rev. B **85**, 184426 (2012).
[17] O.V. Yazyev and A. Pasquarello, Phys. Rev. B **80**, 035408 (2009).
[18] S. Meena and S. Choudhary, AIP Advances **7**, 125008 (2017).

[19] M. Pan, P. Li, W. Qiu, J. Zhao, J. Peng, J. Hu, J. Hu, W. Tian, Y. Hu, D. Chen, X. Wu, Z. Xu, and X. Yuan, Journal of Magnetism and Magnetic Materials **453**, 101 (2018).
[20] V.M. Karpan, P.A. Khomyakov, A.A. Starikov, G. Giovannetti, M. Zwierzycki, M. Talanana, G. Brocks, J. van den Brink, and P.J. Kelly, Phys. Rev. B **78**, 195419 (2008).
[21] G. Kresse and J. Furthmüller, Computational Materials Science **6**, 15 (1996).
[22] G. Kresse and J. Furthmüller, Phys. Rev. B **54**, 11169 (1996).
[23] P.E. Blöchl, Phys. Rev. B **50**, 17953 (1994).
[24] D.M. Ceperley and B.J. Alder, Phys. Rev. Lett. **45**, 566 (1980).
[25] T. Ono and K. Hirose, Phys. Rev. Lett. **82**, 5016 (1999).
[26] T. Ono and K. Hirose, Phys. Rev. B **72**, 085115 (2005).
[27] K. Hirose, T. Ono, and Y. Fujimoto, *First-Principles Calculations In Real-Space Formalism: Electronic Configurations And Transport Properties Of Nanostructures* (Imperial College Pr, London, (2005).
[28] T. Ono, M. Heide, N. Atodiresei, P. Baumeister, S. Tsukamoto, and S. Blügel, Phys. Rev. B **82**, 205115 (2010).
[29] T. Ono and S. Tsukamoto, Phys. Rev. B **93**, 045421 (2016).
[30] J.R. Chelikowsky, N. Troullier, and Y. Saad, Phys. Rev. Lett. **72**, 1240 (1994).
[31] J.R. Chelikowsky, N. Troullier, K. Wu, and Y. Saad, Phys. Rev. B **50**, 11355 (1994).
[32] K. Kobayashi, Computational Materials Science **14**, 72 (1999).
[33] N. Troullier and J.L. Martins, Phys. Rev. B **43**, 1993 (1991).
[34] M. Büttiker, Y. Imry, R. Landauer, and S. Pinhas, Physical Review B **31**, 6207 (1985).
[35] C. Oshima and A. Nagashima, J. Phys.: Condens. Matter **9**, 1 (1997).
[36] C. Yelgel, Journal of Applied Physics **119**, 065307 (2016).
[37] C. Gong, G. Lee, B. Shan, E.M. Vogel, R.M. Wallace, and K. Cho, Journal of Applied Physics **108**, 123711 (2010).

Figure Captions

Figure 1. Schematic illustration of MTJs. (a) symmetric Gr (ML) junction and (b) non-symmetric Gr (ML) junction. (c) Side views of unit-cell showing stacking order at interfaces formed by Co and Ni(111) fcc in combination with Gr ML. Gray balls represent C atoms while red and green balls represent atoms in electrodes. s+1 (s-1) indicates adjacent layer of upper (lower) electrode.

Figure 2. Spin-resolved DOS of ML junctions for lowest-energy structure. (a) Interface layer of Ni or Co electrode, (b) Gr spacer region, (c) interface layer of Ni electrode. (d) Layer-resolved band structure of Gr in symmetric and nnon-symmetric junctions. The electronic contributions of the Gr atoms are projected on the energy bands; where the size of circles is proportional to the degree of the projection and color represents the junction type.

Figure 3. (a) Schematic illustrations of device components for transport calculations. Symmetric Gr ML MTJ is shown as model. Conductance spectra of MTJs. (b) Ni/vacuum/Ni, (c) Co/vacuum/Ni, (d) Ni/Gr(ML)/Ni (e) Co/Gr(ML)/Ni.

Figure 4. 2D-BZ for the rectangular unit cell of Gr. Different k-points of the rectangular unit cell are indicated, while those corresponding to BZ of hexagonal unit cell are indicated by Γ, M and K.

Figure 5. $k_{||} \equiv (k_x , k_y)$ resolved dependence of the conductances of majority-spin in PC.

Figure 6. $k_{||} \equiv (k_x , k_y)$ resolved dependence of the conductances of minority-spin in PC.

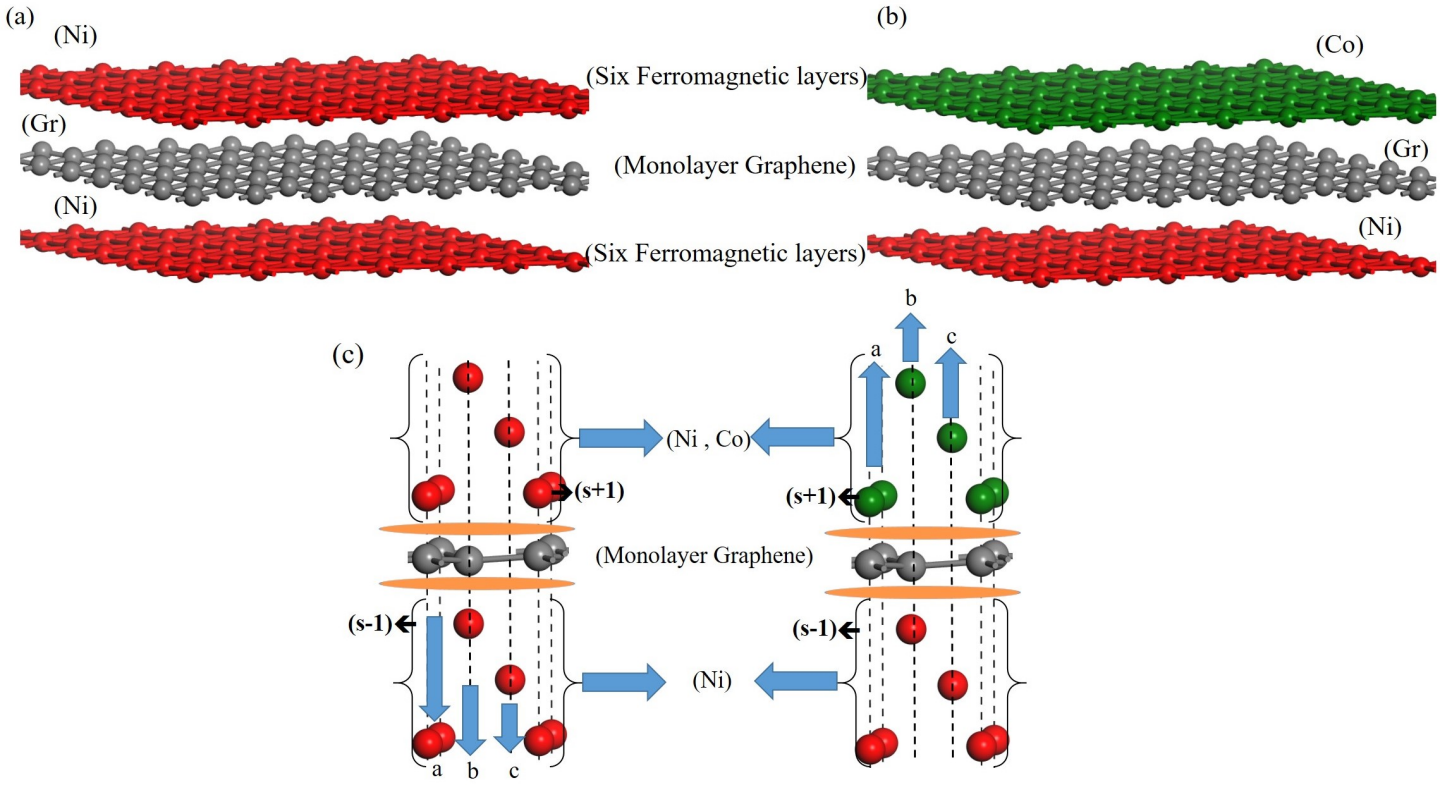
(a)
(Ni)
(Six Ferromagnetic layers)
(Gr)
(Monolayer Graphene)
(Ni)
(Six Ferromagnetic layers)
(b)
(Co)
(Gr)
(Ni)
(c)
(Ni , Co)
(s+1)
(Monolayer Graphene)
(s-1)
(Ni)
a
b
c

Fig. 1

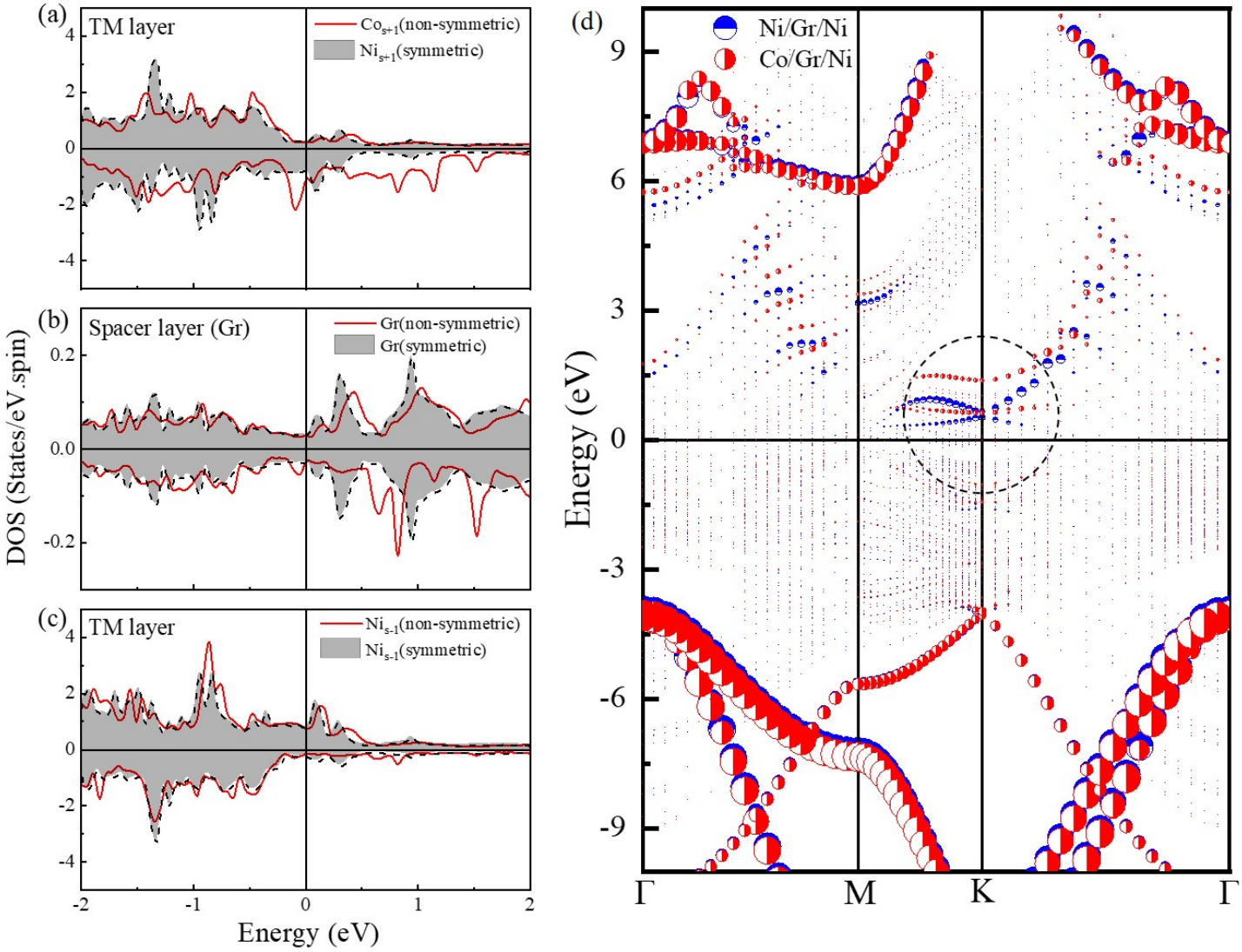
(a)
TM layer
Co$_{s+1}$(non-symmetric)
Ni$_{s+1}$(symmetric)
(b)
Spacer layer (Gr)
Gr(non-symmetric)
Gr(symmetric)
(c)
TM layer
Ni$_{s-1}$(non-symmetric)
Ni$_{s-1}$(symmetric)
DOS (States/eV.spin)
Energy (eV)
(d)
Ni/Gr/Ni
Co/Gr/Ni
Energy (eV)
Γ
M
K
Γ

Fig. 2

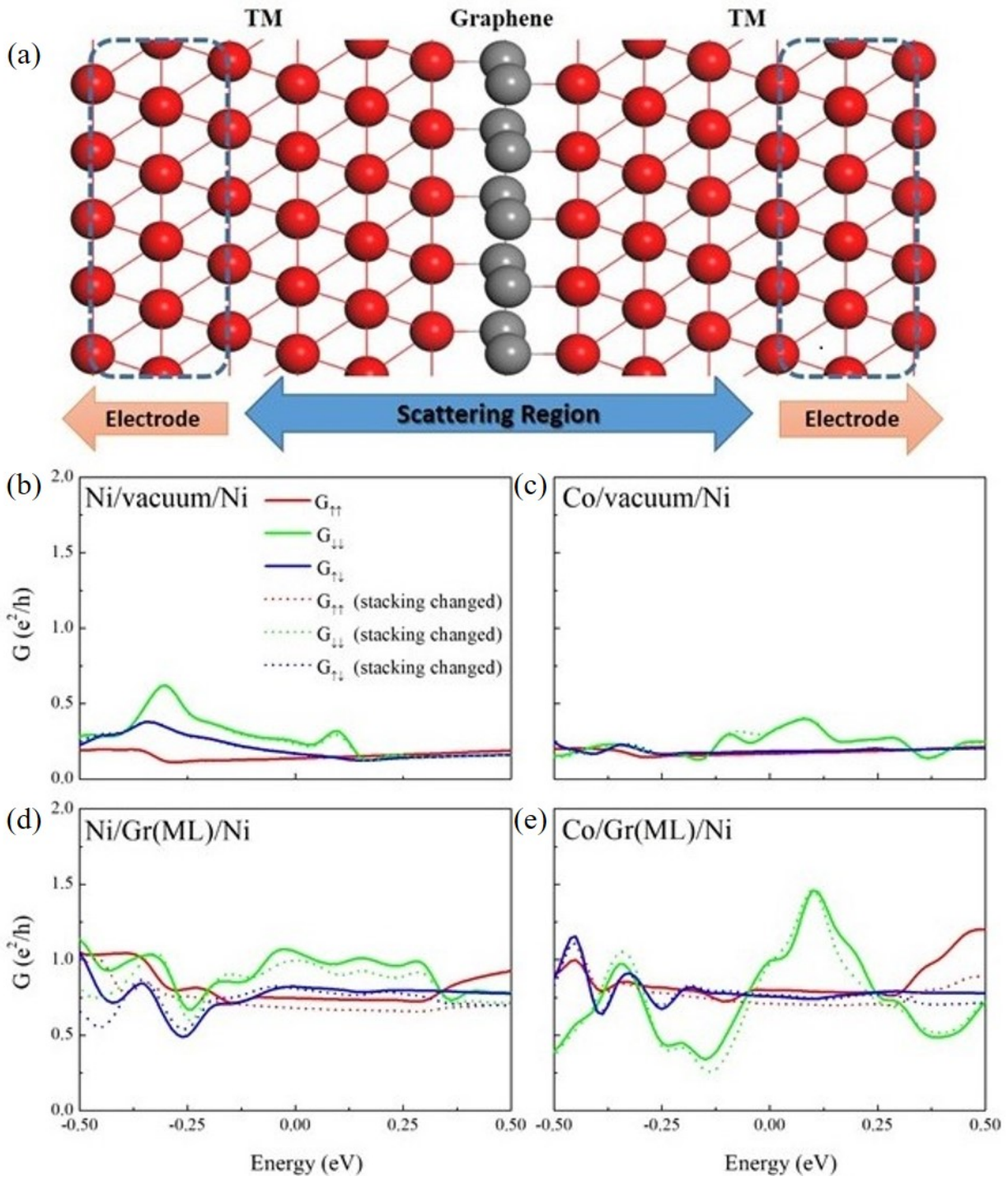
(a)
TM
Graphene
TM
Electrode
Scattering Region
Electrode
(b)
Ni/vacuum/Ni
G↑↑
G↓↓
G↑↓
G↑↑ (stacking changed)
G↓↓ (stacking changed)
G↑↓ (stacking changed)
G (e²/h)
(c)
Co/vacuum/Ni
(d)
Ni/Gr(ML)/Ni
G (e²/h)
Energy (eV)
(e)
Co/Gr(ML)/Ni
Energy (eV)

Fig. 3

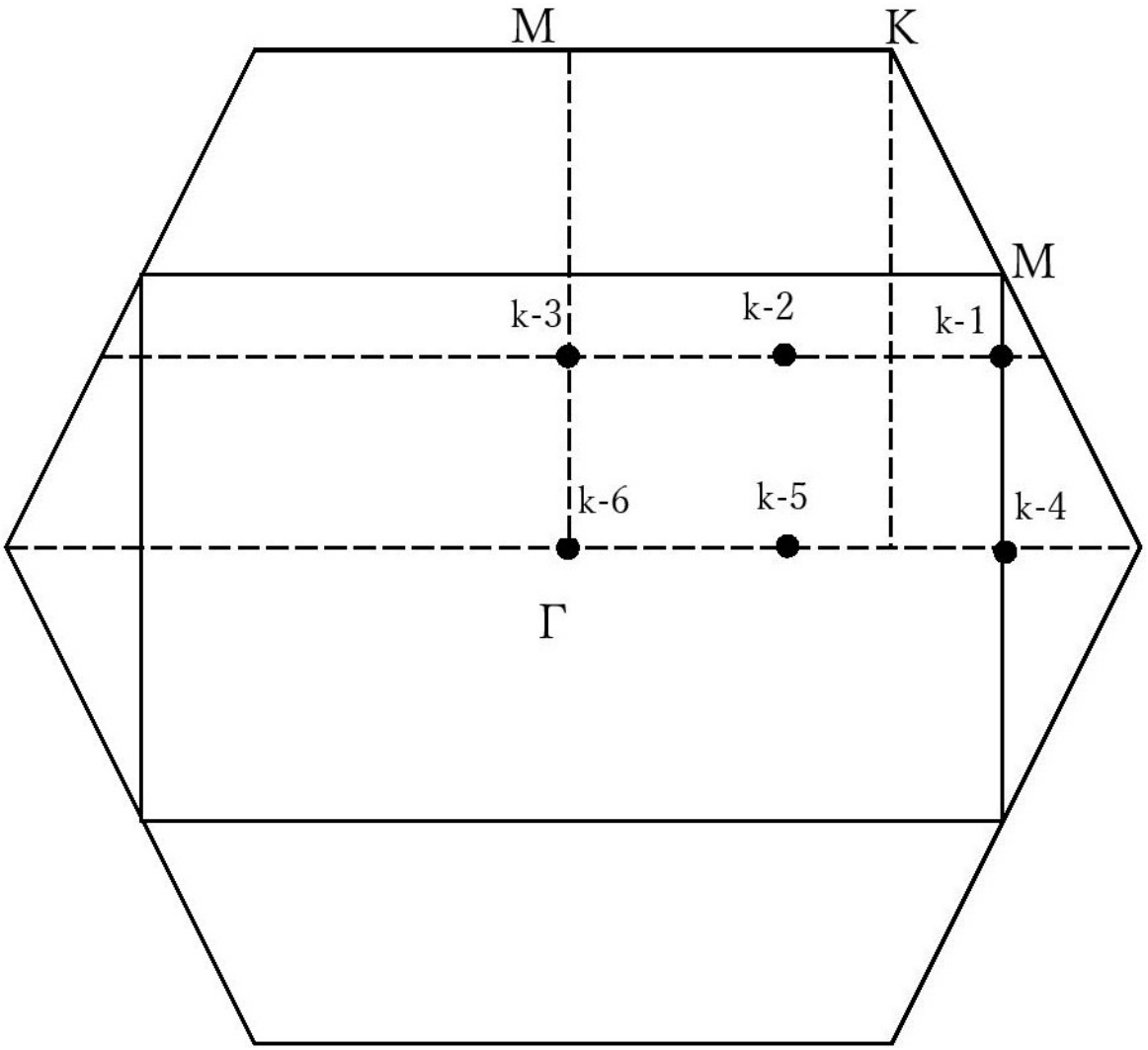

Fig. 4

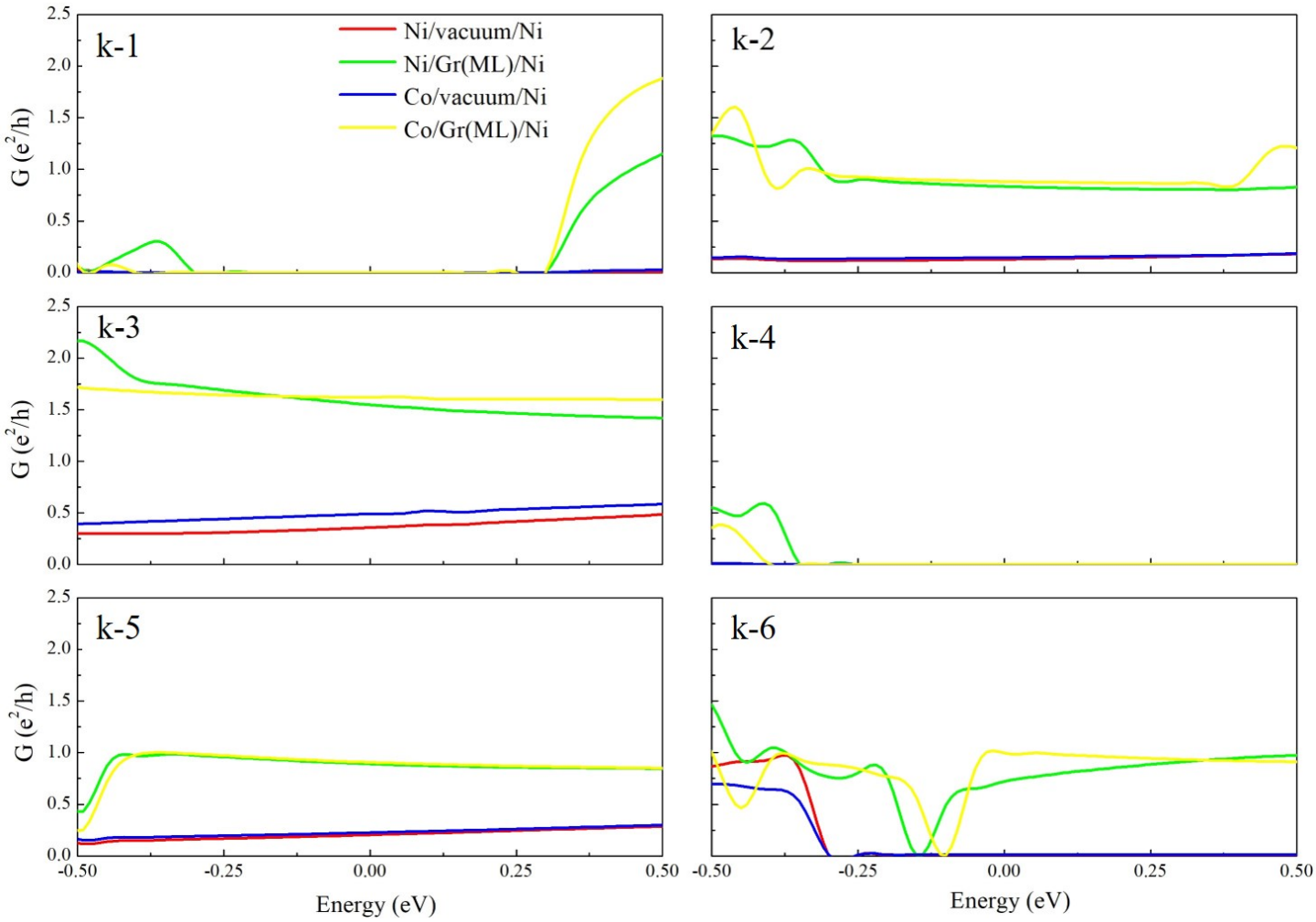
k-1
k-2
k-3
k-4
k-5
k-6
Ni/vacuum/Ni
Ni/Gr(ML)/Ni
Co/vacuum/Ni
Co/Gr(ML)/Ni
G (e²/h)
Energy (eV)
2.5
2.0
1.5
1.0
0.5
0.0
-0.50
-0.25
0.00
0.25
0.50

Fig. 5

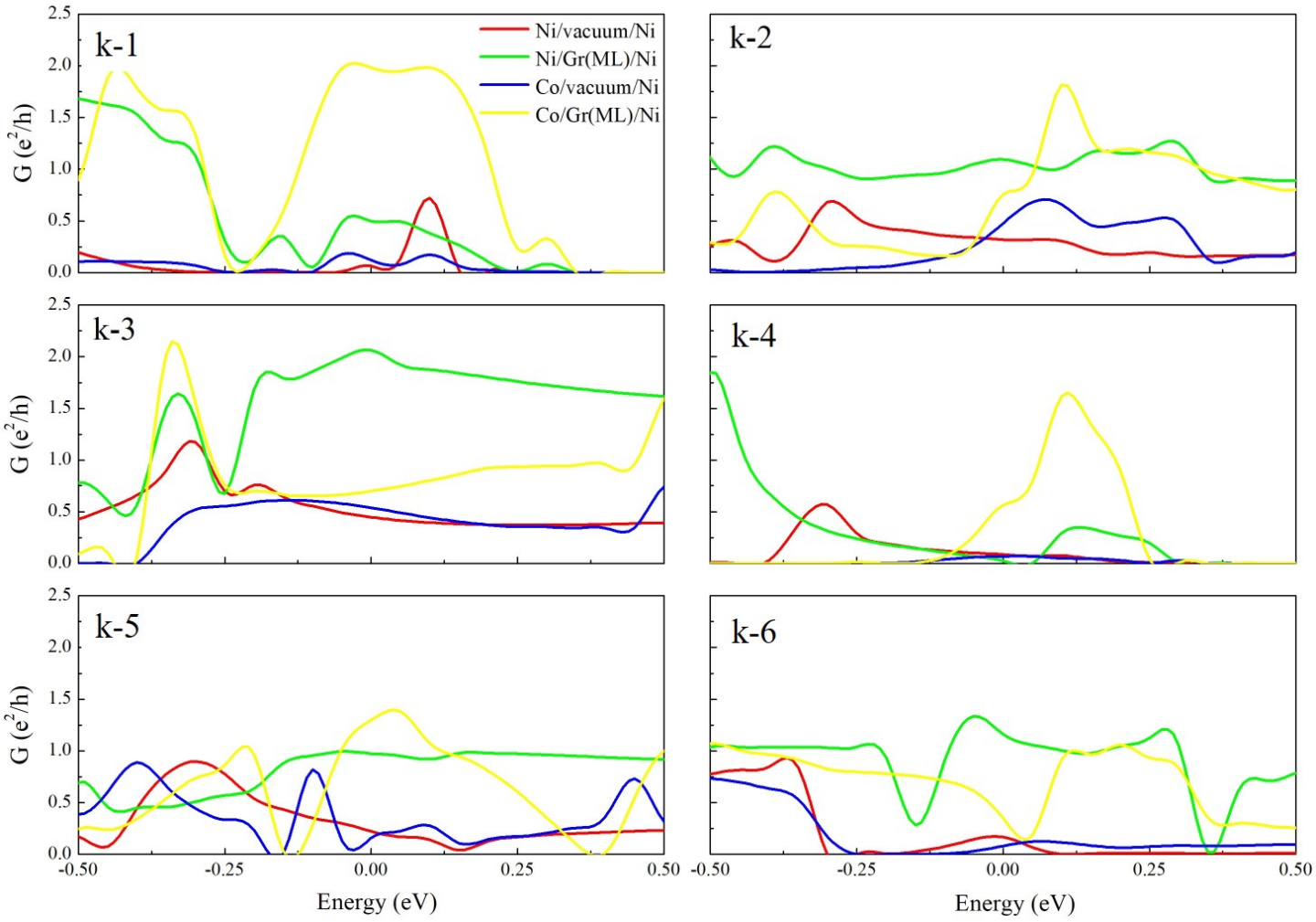
k-1
k-2
k-3
k-4
k-5
k-6
Ni/vacuum/Ni
Ni/Gr(ML)/Ni
Co/vacuum/Ni
Co/Gr(ML)/Ni
G (e²/h)
Energy (eV)
2.5
2.0
1.5
1.0
0.5
0.0
-0.50
-0.25
0.00
0.25
0.50

Fig. 6